inorganics

MDPI

Article

Fluorosolvatochromism of Platinum Supramolecular Coordination Complexes: Stepwise Synthesis and Photophysical Properties of Organometallic Tetranuclear Pt(II) Squares

Antonia Garypidou [1,*], Konstantinos Ypsilantis [1] and Achilleas Garoufis [1,2,*]

[1] Department of Chemistry, University of Ioannina, GR-45110 Ioannina, Greece; k_ipsilantis@yahoo.gr
[2] Institute of Materials Science and Computing, University Research Centre of Ioannina (URCI), GR-45110 Ioannina, Greece
* Correspondence: a.garypidou@uoi.gr (A.G.); agaroufi@uoi.gr (A.G.)

Abstract: The stepwise synthesis and characterization of three new mixed-ligand organometallic tetranuclear platinum squares were achieved. All of the complexes were constituted by the conjunction of two (2,2′-bpy)Pt-terph-Pt(2,2′-bpy) (terph = *p*-terphenyl) fragments linked by a variety of N^N ligands (4,4′-bipyridine (4,4′-bpy), 1,4-di(pyridin-4-yl)benzene (dpbz), and 4,4′-di(pyridin-4-yl)-1,1′-biphenyl (dpbph)), which occupied the fourth coordination site of each metal center, giving rise to square-shaped molecules of the general formula $[Pt_2(2,2'\text{-bpy})_2(\text{terph})(N^{\wedge}N)]_2$. Consequently, the tetranuclear complexes, $\{[Pt(2,2'\text{-bpy})]_4(\mu\text{-terph})_2(\mu\text{-}4,4'\text{-bpy})_2\}\{PF_6\}_4$ (**7**), $\{[Pt(2,2'\text{-bpy})]_4(\mu\text{-terph})_2(\mu\text{-dpbz})_2\}\{PF_6\}_4$ (**8**), and $\{[Pt(2,2'\text{-bpy})]_4(\mu\text{-terph})_2(\mu\text{-dpbph})_2\}\{PF_6\}_4$ (**9**) were constructed. The photophysical properties of these complexes were studied both in the solid state and in various solvents, revealing fluorosolvatochromism.

Keywords: platinum; synthesis; tetranuclear; supramolecular; fluorosolvatochromism

Citation: Garypidou, A.; Ypsilantis, K.; Garoufis, A. Fluorosolvatochromism of Platinum Supramolecular Coordination Complexes: Stepwise Synthesis and Photophysical Properties of Organometallic Tetranuclear Pt(II) Squares. *Inorganics* **2024**, *12*, 132. https://doi.org/10.3390/inorganics12050132

Academic Editor: Rainer Winter

Received: 25 March 2024
Revised: 27 April 2024
Accepted: 28 April 2024
Published: 2 May 2024

1. Introduction

Platinum Supramolecular Coordination Complexes (SCCs) have emerged as attractive subjects of research, garnering significant attention owing to their various properties. They exhibit catalytic specificity in the formation of C-X bonds through reductive elimination [1,2]. Beyond their catalytic potential, platinum squares (a subclass of SCCs with a rectangular shape) have demonstrated noteworthy biological attributes [3] and have been investigated for their promising anticancer properties [4]. Their photophysical properties as dual emitters [5] and fluorescence probes have also been studied.

In recent times, several innovative strategies have been reported for the synthesis of platinum squares, highlighting the dynamic nature of ongoing research in this field. The synthetic strategy commonly involves the one-pot self-assembling of supramolecular units, starting from *cis*-mononuclear building blocks [6–9]. An equal amount of N^N ligands, such as 4,4′-bpy, is then added, resulting in the formation of a symmetric tetranuclear complex.

An alternative synthetic approach involves initially synthesizing one side of the square by forming a binuclear bridged platinum complex. Subsequently, two equivalents of another bridged ligand (BL) coordinate monodentataly to the metal center, resulting in the formation of a "pi" shaped complex. Finally, one more equivalent of the initial binuclear complex completes the fourth side of the square by coordinating the platinum centers to the ends of the BL (Figure 1). This method is known as a stepwise synthesis approach. It is worth noting that the presence of bulky auxiliary ligands on platinum centers, such as bisphosphines, hinders the self-rotation within the binuclear complex, resulting in mixtures of *syn*- and *anti*-conformers. Such mixtures impede the formation of platinum square complexes [10]. Overall, stepwise synthesis offers advantages by enabling the coordination of different types of bridged ligands in the same compound.

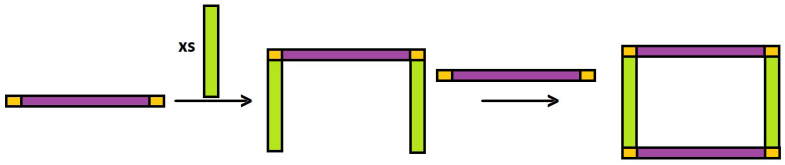

Figure 1. Cartoon representation of stepwise synthesis for a platinum square. The four platinum corners are indicated by a yellow color and the square side ligands by purple and green (BL). The xs of BLs correspond to 10 eq of each BL, as detailed in the experimental section.

In 1990, M. Fujita et al. [11] documented the discovery of tetranuclear square complexes with the synthesis of $[Pd(en)(4,4'\text{-bpy})]_4(NO_3)_8$, prepared through a one-step reaction between the mononuclear complex $Pd(en)(NO_3)_2$ and the ligand 4,4′-bpy. The synthesis of the same complex via a solventless reaction between the same reactants [12] was also reported, suggesting the formation of linear intermediates. Comparative studies revealed that the analogous Pt(II) tetranuclear complex exhibits greater stability than its Pd(II) counterpart, attributed to the higher kinetic inertia of the Pt(II) ion [13]. This Pt(II) complex received significant attention due to its cytotoxic properties against HL-60 cells [14] and its role as a specific G-quadruplex binder [15]. A few years later, Garci et al. reported an alternative synthetic approach for this type of complex utilizing mechanochemical ball milling, forming products in high yields [16].

To date, several Pd(II) tetranuclear complexes have been reported, utilizing various auxiliary ligands such as ethylenediamine [17], 2,2′-bpy and its derivatives [18], and chelated phosphines [19]. Furthermore, tetranuclear rhomboidal Pt(II) complexes have been reported to exhibit aggregation-induced emission properties [20,21]. Also, tunable emission properties were achieved in similar rhomboidal complexes by modifications to the building ligands [22]. The reaction of 2,9-bis[*trans*-$Pt(PEt_3)_2NO_3]_2$(μ-phenanthrene) with rigid dianionic carboxylate ligands affords rhomboid tetranuclear and triangular hexanuclear Pt(II) complexes, depending on the nature of the dicarboxylate ligand [23].

We synthesized and characterized three new mixed-ligand organometallic tetranuclear platinum squares using the stepwise approach. These complexes share a common bridging ligand, *p*-terphenyl (terph), while the other ligands increase in size: 4,4′-bipyridine (4,4′-bpy), 1,4-di(pyridin-4-yl)benzene (dpbz), and 4,4′-di(pyridin-4-yl)-1,1′-biphenyl (dpbph) (Scheme 1). To complete the platinum coordination sphere, we employed 2,2′-bpy as an auxiliary ligand. Thus, the tetranuclear complexes, $\{[Pt(2,2'\text{-bpy})]_4(\mu\text{-terph})_2(\mu\text{-4,4'-bpy})_2\}\{PF_6\}_4$ (**7**), $\{[Pt(2,2'\text{-bpy})]_4(\mu\text{-terph})_2(\mu\text{-dpbz})_2\}\{PF_6\}_4$ (**8**), and $\{[Pt(2,2'\text{-bpy})]_4(\mu\text{-terph})_2(\mu\text{-dpbph})_2\}\{PF_6\}_4$ (**9**) were formed. Our objective was to investigate the photophysical properties of these platinum squares across different solvents.

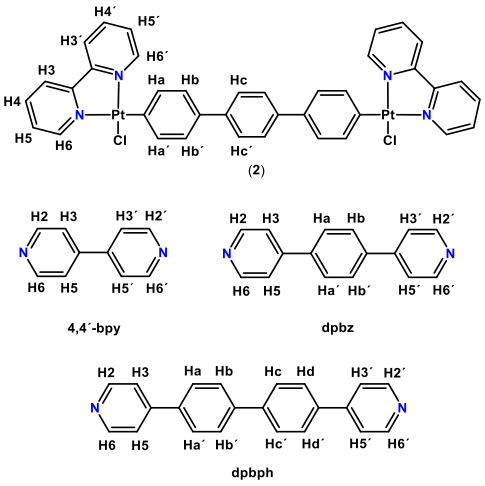

Scheme 1. Numbering and structure of the bimetallic complex (**2**) and the ligands 4,4′-bipyridine, (**4,4′-bpy**), 1,4-di(pyridin-4-yl)benzene, (**dpbz**), and 4,4′-di(pyridin-4-yl)-1,1′-biphenyl, (**dpbph**).

2. Results and Discussion

2.1. Synthesis and Characterization

The synthesis of the complex [Pt(COD)Cl]$_2$(μ-terph) (COD = 1,5-cyclooctadiene) was successfully achieved by modifying the method originally reported for the complex [Pt(COD)Cl]$_2$(μ-bph) [1]. This synthetic procedure (Scheme 2) involved three steps. Firstly, a bromine–lithium exchange reaction was conducted at −78 °C in tetrahydrofuran. Subsequently, 4,4″-bis(trimethylstanyl)-*p*-terphenyl was synthesized in situ after the addition of trimethyltin chloride. Finally, another transmetallation reaction between the arylstannane and the platinum complex Pt(COD)Cl$_2$ resulted in the formation of the binuclear complex (**1**). This binuclear complex served as the starting material for subsequent reactions. In the following step, the coordinated COD in complex (**1**) was replaced by 2,2′-bpy, forming the complex [Pt(2,2′-bpy)Cl]$_2$(μ-terph).

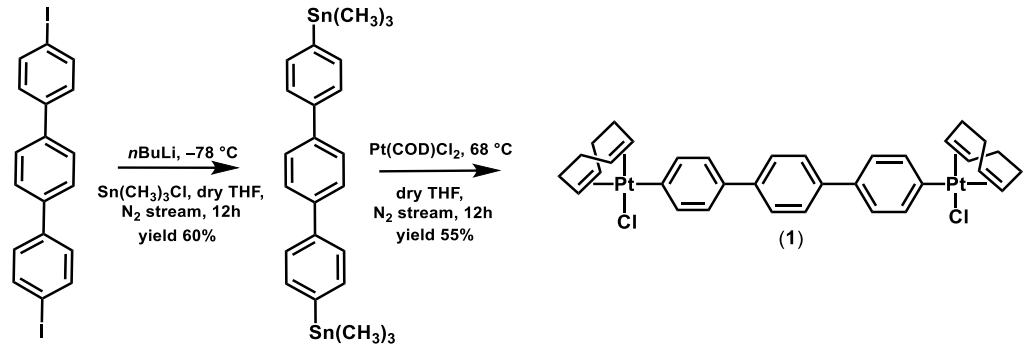

Scheme 2. Synthetic procedure for complex (**1**).

The orientation of the replaceable ligand on the metal center plays a crucial role in facilitating the following reactions. The *anti*-conformer impedes the continuation of the reactions towards the square complex, whereas the *syn*-conformer promotes their formation. Several factors influence this equilibrium, including the steric hindrance by the auxiliary ligands and the rigidity of the bridging ligand [10].

The ^{1}H NMR spectrum of complex (**1**) (Figure S1) in CD_2Cl_2 showed only one set of signals due to its high symmetry. Additionally, it is worth noting that both isomers *syn*- and *anti*-exhibited precisely the same spectrum. In the ^{1}H NMR spectrum of (**2**), the signals of the coordinated 1,5-COD disappeared, indicating that the 1,5-COD was replaced by the ligand 2,2′-bpy in each Pt center (Figure S2). This reaction was accompanied by a noticeable change in the color of the suspended solid from white to bright yellow. Furthermore, the spectrum indicated that the terph exhibited high symmetry, containing two doublets and one singlet peak, all shifted downfield relative to complex (**1**). In contrast, 2,2′-bpy lacked symmetry, exhibiting more than the expected four signals. The presence of double signals attributed to the H6 and H6′, with $\Delta\delta$ = 0.86 ppm, suggested a distinct environment for the two pyridine rings of 2,2′-bpy (Figure S3). In the ROESY spectrum of (**2**) (Figure S4), a cross-peak between H6′ (8.80 ppm) and Ha (7.53 ppm) of terph suggested the proximity of H6′ to the aromatic ring of terph, resulting in a pronounced shielding effect. The signal of H6 appeared significantly downfield, at 9.66 ppm, indicating a strong interaction with the coordinated Cl. This difference was attributed to the orientation of the H6 and H6′ of 2,2′-bpy towards the bridged terph ligand. Also, a significant difference of 0.45 ppm was observed in the H5 and H5′ signals.

Additional evidence supporting the formation of (**2**) was derived from the HR-ESI-MS (Figure S5), where a distinct cluster peak was observed at m/z = 1043.1487. This peak was assigned to the single charged cation $[C_{40}H_{34}N_4ClSO^{195}Pt_2]^+$, which could be formulated as {[Pt$_2$(2,2′-bpy)$_2$(DMSO)Cl](μ-terph)}$^+$. The presence of the DMSO was justified by the preparation of the sample for HR-ESI-MS, where 5 µL of DMSO was added to improve the solubility.

The coordination of the N^N ligands to the platinum center without removing the Cl atoms was not successful. To address this issue, two equivalents of $AgNO_3$ were added (Scheme 3), and the mixture was subjected to sonication using a 750 W equipment. Following the removal of the precipitated AgCl, the complex $\{[Pt(2,2'\text{-bpy})(CH_3CN)]_2(\mu\text{-terph})\}^{2+}$, (**3**) was isolated. The HR-ESI-MS (Figure S6) and NMR spectra confirmed the proposed formula (Figures 2 and S7).

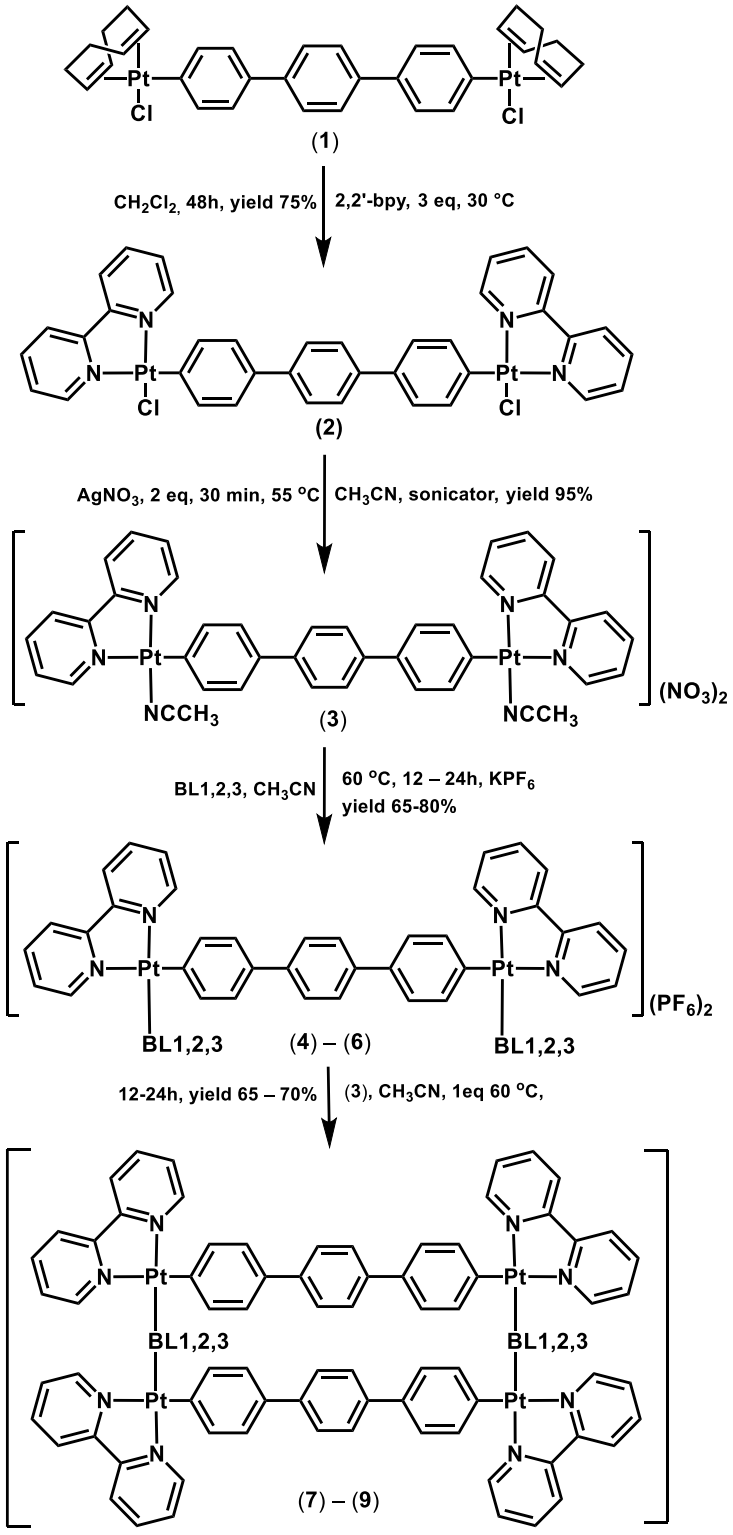

Scheme 3. Synthetic procedure for complexes (**2**)–(**9**).

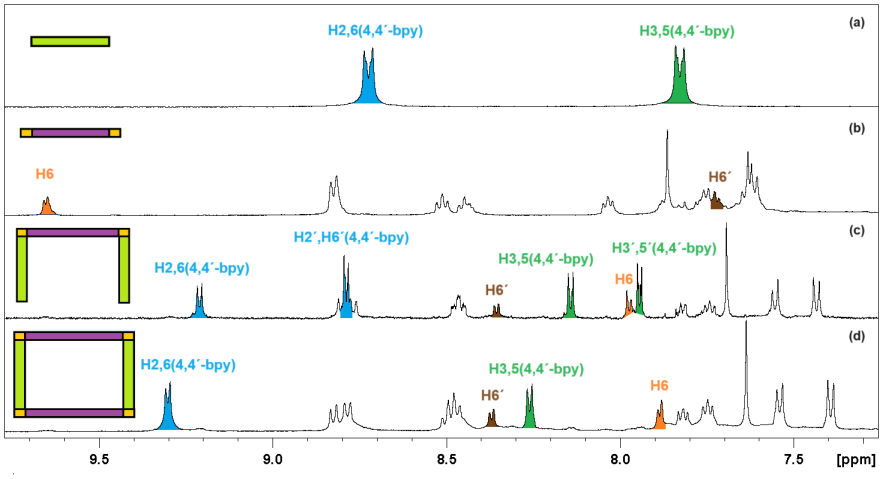

Figure 2. Aromatic region of stacked ^{1}HNMR spectra of 4,4′-bpy (**a**), complex (**3**) (**b**), complex (**4**) (**c**), and complex (**7**) (**d**) in DMSO-d_6 at 500 MHz and 298 K.

Subsequently, the formation of "pi"-shaped complexes (**4**)–(**6**) was achieved by adding an excess of the required BLs (4,4′-bpy, dpbz, dpbph) to act monodentately. This was confirmed by the reduction of the BLs symmetry reflected in the signals of the ^{1}HNMR spectra. Specifically, in ^{1}HNMR of complex (**4**), four signals corresponding to 4,4′-bpy rings were observed (Figure 2). The coordinated pyridine ring showed significant downfield shifts for H6 (+0.60 ppm) and H5 (+0.29 ppm), while the proton signals of the non-coordinated ring shifted slightly downfield. Moreover, upfield shifts were observed for the three signals of terph by 0.3 ppm, probably due to a difference in bond strength between the Pt-Cl and Pt-py. On the other hand, a dramatic upfield shift of 2,2′-bpyH6 by 1.68 ppm was observed, indicating a strong shielding effect. This large shift may be interpreted by the change in the electron density of H6 due to the transition from the Pt-Cl···H6 interaction in (**2**) to the proximity of H6 to the 4,4′-bpy coordinated pyridine ring in (**4**). The other protons of 2,2′-bpy remained almost unaffected after the coordination of 4,4′-bpy.

In the ROESY spectrum of (**4**) (Figure 3), cross-peaks between the H6(2,2′-bpy) → H2/6 (4,4′-bpy), H6′(2,2′-bpy) → Ha(terph), and Ha(terph) → H2/6(4,4′-bpy) confirmed the proposed "pi" shape for this complex. Similar results were observed for all the "pi"-shaped complexes (**4**)–(**6**).

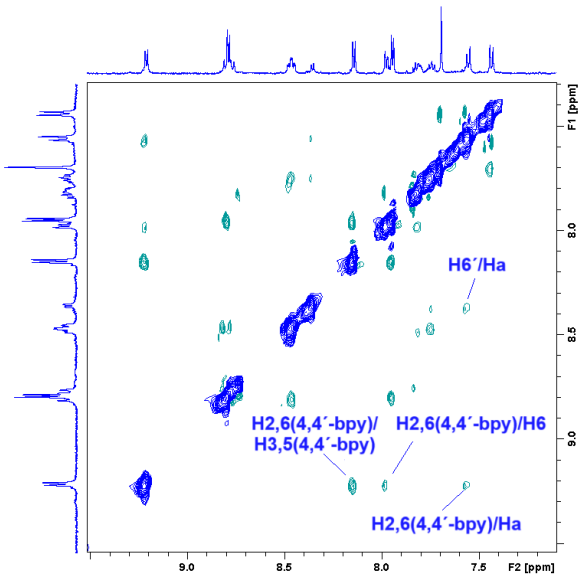

Figure 3. Aromatic region of ^{1}H-^{1}H ROESY spectrum of complex (**4**) in DMSO-d_6 at 298 K in 500 MHz with assignment cross-peaks.

In the ^{1}HNMR spectrum of complex (**7**), the signals that were assigned to the free pyridine rings of 4,4′-bpy were not observed anymore due to their coordination on the Pt(II) centers of the added complex (**3**). Also, complex (**7**) was highly symmetric, resulting in only one set of signals for each ligand (Figure S8). Similar results were also observed for complexes (**8**) and (**9**). At the ROESY spectra of tetranuclear complexes (**7**)–(**9**) (Figures 4 and S9), cross-peaks between 2,2′-bpyH6′ → BLsH2/6, 2,2′-bpyH6 → terphHa, and BLsH2/6 → terphHa were observed. Considering the above constraints on the spatial placing of the ligands (2,2′-bpy, terph, BLs), we concluded that the tetranuclear platinum complexes adopted a rectangular structure.

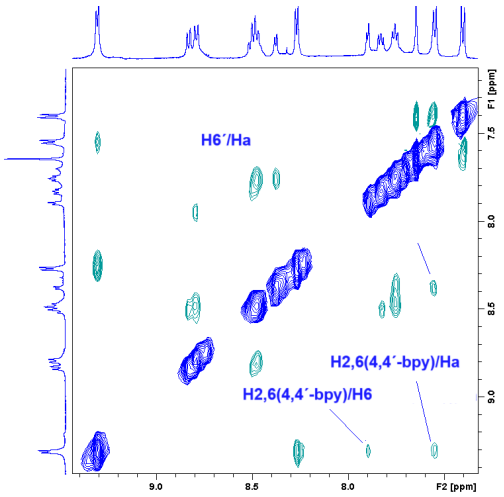

Figure 4. Aromatic region of ^{1}H-^{1}H ROESY spectra of complex (**7**) in DMSO-d$_6$ at 298 K in 500 MHz with assignment at inter-ligand cross-peaks.

The formation and stability of complexes (**7**)–(**9**) were confirmed through HR-ESI mass spectra. Within all spectra, three distinct cluster peaks were observed, corresponding to multicharged cations generated through the successive release of $[PF_6]^-$ ions from the original complex. Consequently, the following cations were assigned: $\{[M]\text{-}4[PF_6]\}^{4+}$, $\{[M]\text{-}3[PF_6]\}^{3+}$, and $\{[M]\text{-}2[PF_6]\}^{2+}$, with $\{[M]\text{-}4[PF_6]\}^{4+}$ being the most predominant among them. The single charged cation $\{[M]\text{-}[PF_6]\}^{+}$ was not observed. The isotopic patterns of these cations closely aligned with the theoretically simulated ones, as illustrated in Figure 5.

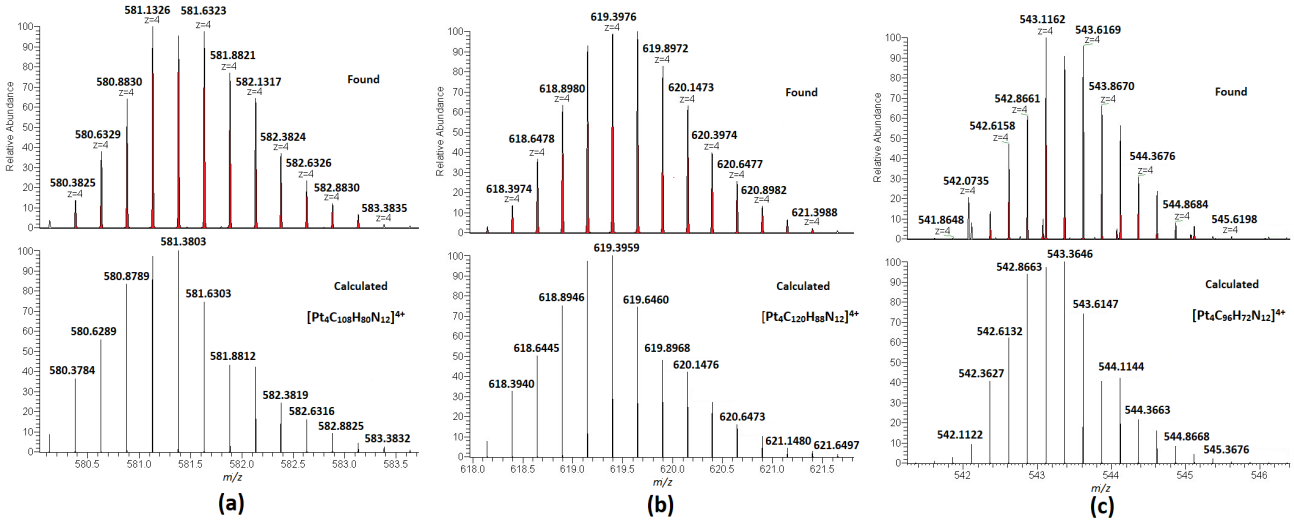

Figure 5. (**a**) HR-ESI MS spectra of complex (**7**) for the cation $\{M\text{-}4[PF_6]\}^{4+}$. (**b**) HR-ESI MS spectra of complex (**8**) for the cation $\{M\text{-}4[PF_6]\}^{4+}$. (**c**) HR-ESI MS spectra of complex (**9**) for the cation $\{M\text{-}4[PF_6]\}^{4+}$.

2.2. Photophysical Studies

2.2.1. Absorption and Emission Spectra of Complexes (**7**)–(**9**)

Table 1 summarizes the photophysical data of complexes (**7**)–(**9**), while Figure 6 illustrates their absorption and emission spectra.

Table 1. Photophysical data of complexes (**7**)–(**9**).

Complex	UV/Vis Absorbance λ_{max} [nm], ($\varepsilon \times 10^4$ [$M^{-1}cm^{-1}$])		Excitation		Emission		QY%	
			λ_{exc}		λ_{em}			
	Solution ($CHCl_3$)	Solid	Solution ($CHCl_3$)	Solid	Solution ($CHCl_3$)	Solid	Solution ($CHCl_3$)	Solid
(**7**)	268 (15.30), 281 (12.2), 328 (5.2)	242, 313, 420	365	400	427	574	1.7%	4%
(**8**)	276 (12.2), 345 (2.1)	242, 315, 418	365	400	433, 615	597	5%	2%
(**9**)	278 (11.1)	242, 313, 422	365	400	431	578	1%	1%

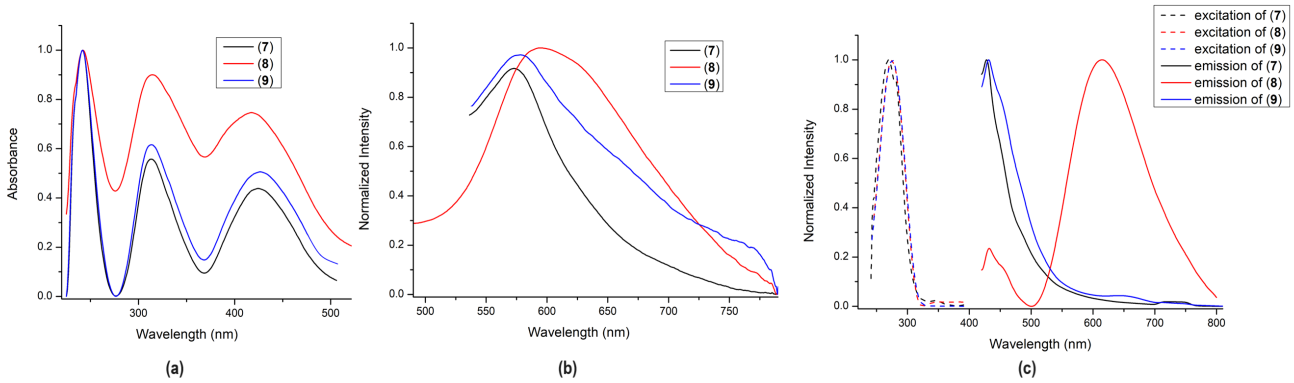

Figure 6. (**a**) Solid-state absorption spectra of complexes (**7**)–(**9**). (**b**) Solid state emission spectra at room temperature of complexes (**7**)–(**9**). (**c**) Excitation and emission spectra of complexes (**7**)–(**9**) in $CHCl_3$ (1.5×10^{-6} M).

The UV–vis spectra of complexes (**7**)–(**9**) in the solid state were similar, while their solution spectra exhibited significant differences from each other. In the solid state, the complexes showed three distinct absorbance bands, two in the UV region and one in the visible region. The absorption bands at 240 nm and 310 nm were attributed to n→π* or π→π* transitions of the aromatic ligands 4,4′-bpy, dpbz, and dpbph. Additionally, the third band observed in the visible region was associated with the metal-to-ligand charge transfer, [(5d)Pt→π*(L)] [24]. However, their absorption spectra in $CHCl_3$ exhibited remarkable differences. Complex (**9**) displayed an intense band at 278 nm assigned to *intra*-ligand transitions arising from their aromatic ring system [25]. In complex (**8**), this band shifted slightly to 276 nm, while, in complex (**7**), it was split to 268 nm and 281 nm, probably due to the differences in the absorption maxima of the containing ligands. A very weak band at 328 nm and 345 nm for complexes (**7**) and (**8**), respectively, was attributed to the [(5d)Pt→π*(L)] transition [24], while it was not observed for complex (**9**) due to its very weak intensity. Similar results have been reported for rhomboidal structures [22], where bands with weak intensity in the range of 420–480 nm were attributed to metal-to-ligand charge transfer [26].

Upon excitation of complexes (**7**)–(**9**) in the solid state with λ_{exc} = 400 nm, emission spectra were obtained, showing a single broad band in the visible region. In complexes (**7**) and (**9**), this band was observed at about 580 nm, while, in complex (**8**), at about 600 nm, each was characterized by low quantum yields. When excited in a dilute solution of $CHCl_3$ at 365 nm, only complex (**8**) demonstrated a strong emission band in the orange part of the spectrum (λ_{em} = 615 nm) accompanied by a weak band at 433 nm. In contrast, complexes

(**7**) and (**9**) exhibited only a single weak band each at 430 nm. Moreover, complex (**8**) demonstrated the highest quantum yield (5%) in $CHCl_3$ compared to complexes (**7**) and (**9**). This complex stood out for its emission at λ_{em} = 615 nm, a feature not yet reported in the literature for this type of tetranuclear platinum square, which typically emits at wavelengths less than 600 nm [20,27].

Furthermore, complex (**8**) could be described as a dual-emitter (615 and 430 nm), a feature that set it apart from the other two complexes (**7**) and (**9**). In general, the dual-emitting effect, arising from distinct excited states [25], could find application in the production of white light [28]. Also, it is worth noting that while some of the literature highlights platinum squares as exceptional emitters, our compounds exhibited lower quantum yields, likely due to the rotational dynamics of phenyl rings leading to fluorescence quenching effects [8,29].

2.2.2. Solvent Effect on Emission Spectra of Complexes (**7**)–(**9**)

The emission spectra of complexes (**7**)–(**9**) were recorded in various solvents (Figure 7 and Table 2), with different polarities to explore their emission profiles. Upon excitation of their solutions at 365 nm, notable distinctions were observed. Specifically, complexes (**7**) and (**9**) in acetone and CH_2Cl_2 exhibited two distinct emission bands: an emission in the blue region and another one in the green (**7**) or red (**9**) region. Also, complex (**9**) exhibited these bands in acetonitrile and ethyl acetate. However, in the other solvents, they showed only a single band in the blue region (420–440 nm), with the exception of the diethyl ether. In diethyl ether, both complexes displayed a shoulder at 450 nm, with complex (**7**) additionally exhibiting a third band at 613 nm. These variations in emission spectra across different solvents highlight the solvent-dependent photophysical behavior of these complexes [21].

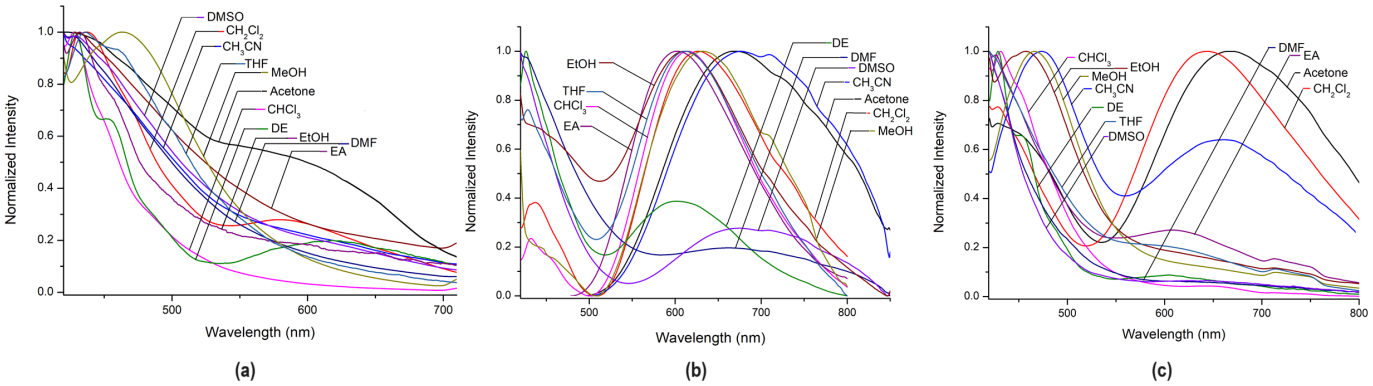

Figure 7. Emission spectra of complexes (**7**) (**a**), (**8**) (**b**), and (**9**) (**c**) in different polarity solvents (λexc. = 365 nm).

Table 2. λ_{em} of complexes (**7**)–(**9**) in solvents with different polarities. DMF: N,N′-dimethylformamide, CH_3CN: acetonitrile, MeOH: methanol, EtOH: ethanol EA: ethyl acetate, THF tetrahydrofuran, DE: diethyl ether.

Complex	Acetone	CH_2Cl_2	CH_3CN	$CHCl_3$	DE	DMF	DMSO	EA	EtOH	MeOH	THF
(**7**)	429 541	437 584	426	427	429 451 613	429	430	431	432	464	436 460
(**8**)	671	436 626	677	433 616	427 605	427 680	421 690	606	429 610	432 632	429 614
(**9**)	433 644	428 642	472 661	431	429 449	421	421	427 616	457	467	421 569

Regarding complex (**8**), notable inconsistencies were evident upon changes in solvents. Specifically, an orange-region band was observed at 605 nm in diethyl ether, while, in DMSO, it shifted closer to the near infra-red region, at 700 nm. In most solvents, excluding acetone, acetonitrile, and ethyl acetate, the complex exhibited two distinct emission bands: one in the blue region and another one in the red-to-orange region. In acetone, acetonitrile, and ethyl acetate, only one orange-red band was observed.

In conclusion, complexes (**7**)–(**9**) demonstrated varying shifts in the emission maxima of their orange-red band across different solvents, a phenomenon commonly referred to as fluorosolvatochromism. However, this magnitude of solvent-dependent variations was not observed for the blue-region band.

3. Experiments

3.1. Materials and Methods

All solvents were of analytical grade and were used without further purification. Tetrahydrofuran (THF) was distilled from sodium benzophenone ketyl, toluene was distilled from CaH_2, and they were stored over molecular sieves. 4,4′-bipyridine, 2,2′-bipyridine, and 1,4-di(pyridin-4-yl)benzene were purchased from Fluorochem, while 4,4′-di(pyridin-4-yl)-1,1′-biphenyl was purchased from TCI. $Pt(COD)Cl_2$, $Sn(CH_3)_3Cl$, and *n*-BuLi (2.5M in hexane) were purchased from Sigma. 4,4″-diiodo-p-terphenyl was synthesized according to the literature [30]. Also, 4,4″-bis(trimethylstannyl)-*p*-terphenyl and $[Pt(COD)Cl]_2$(μ-terph) were synthesized following literature methods [1].

^{1}H NMR spectra for all the compounds were recorded in a Bruker Avance NEO spectrometer operating at 500.13 MHz or in a Bruker Avance II spectrometer operating at 400.13 MHz. The spectra were processed by Topspin 4.2 (Bruker Analytik GmbH, Ettlingen, Germany). Two-dimensional COSY, TOCSY, and ROESY spectra were obtained following standard Bruker procedures. High-resolution electrospray ionization mass spectra (HR-ESI-MS) were recorded using a Thermo Scientific LTQ Orbitrap XL™ system. UV–vis spectra of the complexes were recorded on an Agilent Cary 60 UV–vis spectrophotometer with a xenon source lamp. Sonication of the reaction between $[Pt(bpy)Cl]_2$(μ-terph) and $AgNO_3$ in CH_3CN was accomplished using a Sonics & Materials 750 W instrument (Sonics & Materials, Inc., Leicestershire, UK).

3.2. Fluorescence Emission Studies

Emission studies were conducted using a Jasco FP-8300 fluorometer (Jasco, Tokyo, Japan), which was equipped with a xenon lamp and an integrated sphere for the solid samples. The determination of the relative quantum yield for solutions employed the formula $Qs = Qr(Ar/As)(Es/Er)(ns/nr)^2$. 'A' denotes the absorbance of the solutions, 'E' denotes the integrated fluorescence intensity of the emission spectrum, and 'n' denotes the refractive index of the solvents. Subscripts 'r' and 's' indicate the reference and sample, respectively. A water solution of $[Ru(bpy)_3]Cl_2$ served as the reference standard (Qr = 0.04). The calculation of the relative quantum yield for the complexes in the solid state followed the equation $Q = S_2/(S_0 - S_1)$, where 'Q' denotes the quantum yield of the solid state of the complexes, 'S_2' signifies the integrated emission intensity of the sample, and 'S_0' and 'S_1' refer to the excitation intensities of the standard and the sample, respectively.

*3.3. Synthesis of Complexes (**2**)–(**9**)*

[Pt(2,2′-bpy)Cl]$_2$(μ-terph) (**2**): 56.1 mg of 2,2′-bpy (0.78 mmol) was added to 90 mL of CH_2Cl_2 containing 60 mg (0.059 mmol) of the complex $[Pt(COD)Cl]_2$(μ-terph). The suspension was stirred for about 24 h at 30 °C. After 24 h, the suspension turned into a bright yellow solution. The solvent was evaporated and the solid was washed with hexane and diethyl ether. Yield: 85%. ^{1}H NMR: (500 MHz, 298K, CD_2Cl_2, δ in ppm): H6: 9.66 (d, 2H, ^{3}J = 5.1); H6′: 8.80 (d, 2H, ^{3}J = 5.6); H44′: 8.20 (d, 4H, ^{3}J = 7.6); H3′: 8.17 (t, 2H, ^{3}J = 6.0); H3: 8.10 (t, 2H, ^{3}J = 4.8); H5: 7.79 (t, 2H, ^{3}J = 5.1); Hcc′: 7.77 (s,4H); Haa′: 7.53 (d, 4H, ^{3}J = 8.1); AHbb′: 7.46 (d, 4H, ^{3}J = 8.3); H5′: 7.41 (t, 2H, ^{3}J = 7.0). HR-ESI-MS

(5mL CH_2Cl_2 + 20 μL of DMSO), positive (*m*/*z*): found 1043.1487, calc. 1043.1411 for $[C_{40}H_{34}N_4ClSO^{195}Pt_2]^+$, assignable to the cation $\{[Pt_2(2,2'\text{-bpy})_2(DMSO)Cl](\mu\text{-terph})\}^+$.

{[Pt(2,2′-bpy)(CH$_3$CN)]$_2$(μ-terph)}(NO$_3$)$_2$ (**3**): 11.2 mg of $AgNO_3$ (0.066 mmol) was added to a suspension containing 34 mg (0.033 mmol) of complex (**2**) in 20 mL acetonitrile. The mixture was sonicated for 30 min in 375 W (1/2″ probe) at 55 °C. After sonication, the mixture was filtered and the solvent was evaporated. Yield: 99%. ^{1}H NMR: (500 MHz, 298 K, DMSO-d_6, δ in ppm): H6: 9.65 (d, 2H, ^{3}J = 4.8); H33′: 8.82 (d, 4H, ^{3}J = 8.1); H4: 8.51 (t, 2H, ^{3}J = 8.0); H4′: 8.44 (t, 2H, ^{3}J = 7.8); H5: 8.03 (t, 2H, ^{3}J = 6.6); Hcc′: 7.86 (s, 4H) H6′: 7.75 (d, 2H, ^{3}J = 6.4); H5′: 7.72 (t, 2H, ^{3}J = 5.9); Haa′: 7.64 (d, 4H, ^{3}J = 8.3); Hbb′: 7.61 (d, 4H, ^{3}J = 8.5). HR-ESI-MS (CH_3CN), positive (*m*/*z*): found 506.1066, calc. 506.1058 for $[C_{42}H_{34}N_6{}^{195}Pt_2]^{2+}$, assignable to the cation $\{[Pt(2,2'\text{-bpy})(CH_3CN)]_2(\mu\text{-terph})\}^{2+}$.

{[Pt(2,2′-bpy)(4,4′-bpy)]$_2$(μ-terph)}(PF$_6$)$_2$ (**4**): 46.3 mg (0.29 mmol) of 4,4′-bpy was added to 50 mL acetonitrile containing 30 mg (0.029 mmol) of complex (**3**) {[Pt(2,2′-bpy)(CH_3CN)](μ-terph)}{NO_3}$_2$ and 10.7 mg (0.058) mmol of KPF_6. The mixture was stirred for 18 h at room temperature. After the evaporation of the solvent, the orange solid was washed with H_2O and diethyl ether. Yield: 60%. ^{1}H NMR: (500 MHz, 298 K, DMSO-d_6, δ in ppm): H26(4,4′-bpy): 9.21 (d, 4H, ^{3}J = 6.9); H3′: 8.80 (d, 2H, ^{3}J = 8.4); H2′6′(4,4′-bpy): 8.78 (d, 4H, ^{3}J = 6.2); H3: 8.76 (d, 2H, ^{3}J = 8.0); H44′: 8.46 (t, 4H, ^{3}J = 7.6); H6′: 8.35 (d, 2H, ^{3}J = 5.9); H35(4,4′-bpy): 8.14 (d, 4H, ^{3}J = 5.9); H6: 7.97 (d, 2H, ^{3}J = 6.0); H3′5′(4,4′-bpy): 7.94 (d, 4H, ^{3}J = 5.9); H5: 7.82 (t, 2H, ^{3}J = 6.2); H5′: 7.74 (t, 2H, ^{3}J = 6.7); Hcc′: 7.69 (s,4H); Haa′: 7.55 (d, 4H, ^{3}J = 8.2); Hbb′: 7.43 (d, 4H, ^{3}J = 8.2).

{[Pt(2,2′-bpy)(dpbz)]$_2$(μ-terph)}(PF$_6$)$_2$ (**5**): 67.3 mg (0.29 mmol) of dpbz was added to 40 mL acetonitrile containing 30 mg (0.029 mmol) of complex (**2**) {[Pt(2,2-bpy)(CH_3CN)](μ-terph)}{NO_3}$_2$ and 10.7 mg (0.058) mmol of KPF_6. The mixture was stirred for 22 h at room temperature. After the evaporation of the solvent, the orange solid was washed with acetone and diethyl ether. Yield: 75%. ^{1}H NMR: (500 MHz, 298 K, DMSO-d_6, δ in ppm): H26(dpbz): 9.06 (d, 4H, ^{3}J = 6.4); H3′: 8.71 (d, 2H, ^{3}J = 7.5); H2′6′(dpbz): 8.68 (d, 4H, ^{3}J = 6.0); H3: 8.66 (d, 2H, ^{3}J = 8.6); H44′: 8.49 (t, 4H, ^{3}J = 7.9); H6′: 8.35 (d, 2H, ^{3}J = 5.9); H35(dpbz): 8.21 (d, 4H, ^{3}J = 6.6); Haa′bb′(dpbz): 8.28 (s,8H); H6: 8.21 (d, 2H, ^{3}J = 6.1); H3′5′(dpbz): 8.15 (d, 4H, ^{3}J = 6.8); H5: 8.03 (t, 2H, ^{3}J = 7.1); H5′: 7.98 (t, 2H, ^{3}J = 7.2); Hcc′: 7.69 (s,4H); Haa′: 7.58 (d, 4H, ^{3}J =7.5); AHbb′: 7.46 (d, 4H, ^{3}J = 7.87).

{[Pt(2,2′-bpy)(dpbph)]$_2$(μ-terph)}(PF$_6$)$_2$ (**6**): 90.5 mg (0.29 mmol) of dpbph was added to 70 mL acetonitrile containing 30 mg (0.029 mmol) of complex (**2**) {[Pt(2,2-bpy)(CH_3CN)](μ-terph)}{NO_3}$_2$ and 10.7 mg (0.058) mmol of KPF_6. The mixture was stirred for 24 h at room temperature. After the evaporation of the solvent, the orange solid was washed with THF and diethyl ether. Yield: 55%. ^{1}H NMR: (500 MHz, 298 K, DMSO-d_6, δ in ppm): H26(dpbph): 8.98 (d, 4H, ^{3}J = 7.2); H2′6′(dpbph): 8.89 (d, 4H, ^{3}J = 6.8); H3′: 8.88 (d, 2H, ^{3}J = 7.6); H3: 8.87 (d, 2H, ^{3}J = 7.1); H44′: 8.43 (t, 4H, ^{3}J = 7.2); H6′: 8.27 (d, 2H, ^{3}J = 6.1); H35(dpbph): 8.01 (d, 4H, ^{3}J = 6.9); H6: 7.97 (d, 2H, ^{3}J = 6.9); Haa′bb′cc′(dpbph): 7.92 (dd, 8H, ^{3}J = 6.5); H5: 7.82 (t, 2H, ^{3}J = 6.2); H5′: 7.75 (t, 2H, ^{3}J = 7.2); Hcc′: 7.65 (s, 8H); AHaa′: 7.49 (d, 4H, ^{3}J = 8.4); AHbb′: 7.35 (d, 4H, ^{3}J = 8.2).

The tetranuclear Pt(II) complexes (**7**)–(**9**) were synthesized similarly. In a typical experiment, 1 eq. of complex (**3**) was added to 20–30 mL acetonitrile containing 1 eq. of the binuclear complexes (**4**)–(**6**). The mixture was heated for 20–25 h at 60 °C. After 19 h, the reaction mixture was evaporated to dryness under reduced pressure and the orange solid was washed several times with dichloromethane and diethyl ether.

{[Pt(2,2′-bpy)]$_4$(μ-terph)$_2$(μ-(4,4′-bpy)$_2$}(PF$_6$)$_4$ (**7**): 3.4 mg (0.020 mmol) of 4,4′-bpy was added to 20 mL acetonitrile containing 32 mg (0.020 mmol) of complex (**4**). Yield: 55%. ^{1}HNMR: (500 MHz, 298 K, DMSO-d_6, δ in ppm): H26(4,4′-bpy): 9.30 (d, 8H, ^{3}J = 6.5); H3′: 8.82 (d, 4H, ^{3}J = 8.4); H3: 8.78 (d, 4H, ^{3}J = 8.5); H44′: 8.48 (tt, 8H, ^{3}J = 7.6); H6′: 8.37 (d, 4H, ^{3}J = 6.0); H35(4,4′-bpy): 8.26 (d, 8H, ^{3}J = 6.9); H6: 7.88 (d, 4H, ^{3}J = 4.9); H5: 7.81 (t, 4H, ^{3}J = 7.1); H5′: 7.74 (t, 4H, ^{3}J = 6.7); Hcc′: 7.63 (s, 8H); Haa′: 7.54 (d, 8H, ^{3}J = 8.1); Hbb′: 7.39 (d, 8H, ^{3}J = 8.3). HR-ESI-MS, positive (*m*/*z*): found 543.3665, calc. 543.3646

for $[C_{96}H_{72}N_{12}{}^{195}Pt_4]^{4+}$; found 772.8104, calc. 772.8078 for $[C_{96}H_{72}N_{12}PF_6{}^{195}Pt_4]^{3+}$; found 1231.6974, calc. 1231.6940 for $[C_{96}H_{72}N_{12}P_2F_{12}{}^{195}Pt_4]^{2+}$.

{[Pt^{II}(2,2′-bpy)]$_4$(μ-terph)$_2$(μ-dpbz)$_2$}{PF$_6$}$_4$ (**8**): 3.2 mg (0.013 mmol) of dpbz was added to 20 mL acetonitrile containing 5 mg (0.013 mmol) of complex (**5**). Yield: 68%. ^{1}HNMR: (500 MHz, 298K, DMSO-d$_6$, δ in ppm): H26(dpbz): 9.14 (d, 8H, ^{3}J = 6.7); H3: 8.81 (d, 4H, ^{3}J = 8.3); H3′: 8.77 (d, 4H, ^{3}J = 8.6); H44′: 8.47 (tt, 8H, ^{3}J = 7.0); H6′: 8.37 (d, 4H, ^{3}J = 5.7); Haa′bb′(dpbz): 8.16 (s, 8H); H35(dpbz): 8.13 (s, 4H); H6: 7.99 (d, 8H, ^{3}J = 5.6); H5: 7.81 (t, 4H, ^{3}J = 6.7); H5′: 7.74 (t, 4H, ^{3}J = 6.8); Hcc′: 7.67 (s, 8H); Haa′: 7.56 (d, 8H, ^{3}J = 8.1); Hbb′: 7.43 (d, 8H, ^{3}J = 8.4). HR-ESI-MS, positive (m/z): found 581.3825, calc. 581.3803 for $[C_{108}H_{80}N_{12}{}^{195}Pt_4]^{4+}$; found 823.4971, calc. 823.4953 for $[C_{108}H_{80}N_{12}PF_6{}^{195}Pt_4]^{3+}$.

{[Pt^{II}(2,2′-bpy)]$_4$(μ-terph)$_2$(μ-dpbph)$_2$}{PF$_6$}$_4$ (**9**): 5.1 mg (0.016 mmol) of dpbph was added to 30 mL acetonitrile containing 31 mg (0.016mmol) of complex (**6**). Yield: 50%. ^{1}HNMR: (500 MHz, 298 K, DMSO-d$_6$, δ in ppm): H26(dpbph): 9.10 (d, 8H, ^{3}J = 6.1); H3: 8.81 (d, 4H, ^{3}J = 8.2); H3′: 8.77 (d, 4H, ^{3}J = 8.4); H44′: 8.47 (t, 4H, ^{3}J = 8.4); H6′: 8.38 (d, 4H, ^{3}J = 5.8); H35(dpbph): 8.09 (dd, 8H, ^{3}J = 6.8); Haa′bb′(dpbph): 8.08 (dd, 8H, ^{3}J = 7.3); H6: 8.02 (d, 4H, ^{3}J = 5.0); H5: 7.83 (t, 4H, ^{3}J = 7.5); H5′: 7.75 (t, 4H, ^{3}J = 6.3); Hcc′: 7.70 (s, 8H); Haa′: 7.56 (d, 8H, ^{3}J = 8.1); Hbb′: 7.45 (d, 8H, ^{3}J = 8.2). HR-ESI-MS, positive (m/z): found 619.3976, calc. 619.3959 for $[C_{120}H_{88}N_{12}{}^{195}Pt_4]^{4+}$; found 874.1847, calc. 874.1828 for $[C_{120}H_{88}N_{12}PF_6{}^{195}Pt_4]^{3+}$.

4. Conclusions

In conclusion, the tetranuclear complexes {[Pt(2,2′-bpy)]$_4$(μ-terph)$_2$(μ-4,4′-bpy)$_2$}{PF$_6$}$_4$ (**7**), {[Pt(2,2′-bpy)]$_4$(μ-terph)$_2$(μ-dpbz)$_2$}{PF$_6$}$_4$ (**8**), and {[Pt(2,2′-bpy)]$_4$(μ-terph)$_2$(μ-dpbph)$_2$}{PF$_6$}$_4$ (**9**) were synthesized through a stepwise method and characterized by NMR and HR-ESI mass spectrometry. The photophysical properties of these complexes were investigated both in the solid state and in various solvents. All complexes, (**7**)–(**9**), displayed solvent-dependent photophysical behavior, altering their emissions based on the solvent, a phenomenon known as fluorosolvatochromism. Complex (**8**) demonstrated a pronounced dependence of the emission λ_{max} on the polarity [31] of several solvents used, DMSO ≈ DMF ≈ CH_3CN > Acetone > CH_2Cl_2 > $CHCl_3$ > EA ≈ DE, following the general trend of increasing λ_{max} by the increase in solvent polarity.

Supplementary Materials: The following supporting information can be downloaded at https://www.mdpi.com/article/10.3390/inorganics12050132/s1: Figure S1: ^{1}HNMR of complex [Pt(COD)Cl]$_2$(μ-terph) (**1**) in CD_2Cl_2 in 500 MHz 298 K. Figure S2: Aromatic region of ^{1}HNMR of complex [Pt(2,2′-bpy)Cl]$_2$(μ-terph) (**2**) in CD_2Cl_2 in 500 MHz 298 K. Figure S3: Aromatic region of ^{1}H-^{1}H COSY spectrum of complex [Pt(2,2′-bpy)Cl]$_2$(μ-terph) (**2**) in CD_2Cl_2 in 500 MHz 298 K with assignment cross-peaks. Figure S4: Aromatic region of ^{1}H-^{1}H ROESY spectrum of complex (**2**) in CD_2Cl_2 in 500 MHz 298 K with assignment cross-peaks. Figure S5: HR-ESI MS spectrum of complex [Pt(2,2′-bpy)Cl]$_2$(μ-terph) (**2**). Figure S6: HR-ESI MS spectrum of complex {[Pt(2,2′-bpy)(CH_3CN)]$_2$(μ-terph)}(NO_3)$_2$ (**3**). Figure S7: Aromatic region of ^{1}H-^{1}H COSY (a) and ^{1}H-^{1}H TOCSY (b) spectra of complex {[Pt(2,2′-bpy)(CH_3CN)]$_2$(μ-terph)}(NO_3)$_2$ (**3**) in DMSO-d$_6$ in 500 MHz 298 K with assignment cross-peaks. Figure S8: Aromatic region of ^{1}H-^{1}H COSY (a) and ^{1}H-^{1}H TOCSY(b) spectra of complex {[Pt(2,2′-bpy)]$_4$(μ-terph)$_2$(μ-(4,4′-bpy)$_2$}{PF$_6$}$_4$ (**7**) in DMSO-d$_6$ in 500 MHz 298 K with assignment cross-peaks. Figure S9: Aromatic region of ^{1}H-^{1}H ROESY spectra of complexes (**8**) (a) and (**9**) (b) in DMSO-d$_6$ at 298 K in 500 MHz with assignment at inter-ligand cross-peaks.

Author Contributions: Conceptualization, methodology, validation, investigation, writing—original draft preparation, writing—review and editing, A.G. (Antonia Garypidou); Conceptualization, methodology, K.Y.; Conceptualization, writing—original draft preparation, writing—review and editing, supervision, A.G. (Achilleas Garoufis). All authors have read and agreed to the published version of the manuscript.

Funding: This research received no external funding.

Data Availability Statement: Data are contained within the article and supplementary materials.

Acknowledgments: We acknowledge the Unit of Environmental, Organic and Biochemical for the high-resolution analysis of ORBITRAP-LC-MS, the X-ray Center for single-crystal diffraction, and the NMR Centre of the University of Ioannina for providing access to the facilities.

Conflicts of Interest: The authors declare no conflicts of interest.

References

1. Iwamoto, T.; Watanabe, Y.; Sakamoto, Y.; Suzuki, T.; Yamago, S. Selective and Random Syntheses of [n]Cycloparaphenylenes (n = 8–13) and Size Dependence of Their Electronic Properties. *J. Am. Chem. Soc.* **2011**, *133*, 8354–8361. [CrossRef] [PubMed]
2. Vivekananda, K.V.; Dey, S.; Maity, D.K.; Bhuvanesh, N.; Jain, V.K. Supramolecular Macrocyclic Pd(II) and Pt(II) Squares and Rectangles with Aryldithiolate Ligands and Their Excellent Catalytic Activity in Suzuki C–C Coupling Reaction. *Inorg. Chem.* **2015**, *54*, 10153–10162. [CrossRef] [PubMed]
3. Zheng, X.H.; Chen, H.Y.; Tong, M.L.; Ji, L.N.; Mao, Z.W. Platinum Squares with High Selectivity and Affinity for Human Telomeric G-Quadruplexes. *Chem. Commun.* **2012**, *48*, 7607–7609. [CrossRef] [PubMed]
4. Grishagin, I.V.; Pollock, J.B.; Kushal, S.; Cook, T.R.; Stang, P.J.; Olenyuk, B.Z. In Vivo Anticancer Activity of Rhomboidal Pt(II) Metallacycles. *Proc. Natl. Acad. Sci. USA* **2014**, *111*, 18448–18453. [CrossRef] [PubMed]
5. Garypidou, A.; Ypsilantis, K.; Plakatouras, J.C.; Garoufis, A. Dual-Emissive Rectangular Supramolecular Pt(II)-p-Biphenyl with 4,4′-Bipyridine Derivative Metallacycles: Stepwise Synthesis and Photophysical Properties. *Molecules* **2023**, *28*, 7261. [CrossRef] [PubMed]
6. Sinha, N.; Roelfes, F.; Hepp, A.; Hahn, F.E. Single-Step Synthesis of Organometallic Molecular Squares from NR,NR′,NR′′,NR′′′-Substituted Benzobiscarbenes. *Chem. A Eur. J.* **2017**, *23*, 5939–5942. [CrossRef] [PubMed]
7. Würthner, F.; Sautter, A. Highly Fluorescent and Electroactive Molecular Squares Containing Perylene Bisimide Ligands. *Chem. Commun.* **2000**, *2*, 445–446. [CrossRef]
8. Chen, J.-S.; Zhao, G.-J.; Cook, T.R.; Han, K.-L.; Stang, P.J. Photophysical Properties of Self-Assembled Multinuclear Platinum Metallacycles with Different Conformational Geometries. *J. Am. Chem. Soc.* **2013**, *135*, 6694–6702. [CrossRef]
9. Goeb, S.; Bivaud, S.; Dron, P.I.; Balandier, J.Y.; Chas, M.; Sallé, M. A Bpttf-Based Self-Assembled Electron-Donating Triangle Capable of C60 Binding. *Chem. Commun.* **2012**, *48*, 3106–3108. [CrossRef]
10. Schmidtendorf, M.; Pape, T.; Hahn, F.E. Molecular Rectangles from Platinum(Ii) and Bridging Dicarbene, Diisocyanide and 4,4′-Bipyridine Ligands. *Dalt. Trans.* **2013**, *42*, 16128–16141. [CrossRef] [PubMed]
11. Fujita, M.; Yazaki, J.; Ogura, K. Preparation of a Macrocyclic Polynuclear Complex, [(En)Pd(4,4′-Bpy)]4(NO3)8 (En = Ethylenediamine, Bpy = Bipyridine), Which Recognizes an Organic Molecule in Aqueous Media. *J. Am. Chem. Soc.* **1990**, *112*, 5645–5647. [CrossRef]
12. Orita, A.; Jiang, L.; Nakano, T.; Ma, N.; Otera, J. Solventless Reaction Dramatically Accelerates Supramolecular Self-Assembly. *Chem. Commun.* **2002**, *2*, 1362–1363. [CrossRef]
13. Würthner, F.; You, C.-C.; Saha-Möller, C.R. Metallosupramolecular Squares: From Structure to Function. *Chem. Soc. Rev.* **2004**, *33*, 133–146. [CrossRef] [PubMed]
14. Mounir, M.; Lorenzo, J.; Ferrer, M.; Prieto, M.J.; Rossell, O.; Avilès, F.X.; Moreno, V. DNA Interaction and Antiproliferative Behavior of the Water Soluble Platinum Supramolecular Squares [(En)Pt(N–N)]4(NO3)8 (En=ethylenediamine, N–N=4,4′-Bipyridine or 1,4-Bis(4-Pyridyl)Tetrafluorobenzene). *J. Inorg. Biochem.* **2007**, *101*, 660–666. [CrossRef] [PubMed]
15. Kieltyka, R.; Englebienne, P.; Fakhoury, J.; Autexier, C.; Moitessier, N.; Sleiman, H.F. A Platinum Supramolecular Square as an Effective G-Quadruplex Binder and Telomerase Inhibitor. *J. Am. Chem. Soc.* **2008**, *130*, 10040–10041. [CrossRef] [PubMed]
16. Garci, A.; Castor, K.J.; Fakhoury, J.; Do, J.L.; Di Trani, J.; Chidchob, P.; Stein, R.S.; Mittermaier, A.K.; Friščić, T.; Sleiman, H. Efficient and Rapid Mechanochemical Assembly of Platinum(II) Squares for Guanine Quadruplex Targeting. *J. Am. Chem. Soc.* **2017**, *139*, 16913–16922. [CrossRef]
17. Chand, D.K.; Biradha, K.; Kawano, M.; Sakamoto, S.; Yamaguchi, K.; Fujita, M. Dynamic Self-Assembly of an M 3 L 6 Molecular Triangle and an M 4 L 8 Tetrahedron from Naked Pd II Ions and Bis(3-pyridyl)-Substituted Arenes. *Chem. An Asian J.* **2006**, *1*, 82–90. [CrossRef] [PubMed]
18. Ning, G.-H.; Yao, L.-Y.; Liu, L.-X.; Xie, T.-Z.; Li, Y.-Z.; Qin, Y.; Pan, Y.-J.; Yu, S.-Y. Self-Assembly and Host−Guest Interaction of Metallomacrocycles Using Fluorescent Dipyrazole Linker with Dimetallic Clips. *Inorg. Chem.* **2010**, *49*, 7783–7792. [CrossRef] [PubMed]
19. You, C.; Hippius, C.; Grüne, M.; Würthner, F. Light-Harvesting Metallosupramolecular Squares Composed of Perylene Bisimide Walls and Fluorescent Antenna Dyes. *Chem. A Eur. J.* **2006**, *12*, 7510–7519. [CrossRef] [PubMed]
20. Chen, L.; Chen, C.; Sun, Y.; Lu, S.; Huo, H.; Tan, T.; Li, A.; Li, X.; Ungar, G.; Liu, F.; et al. Luminescent Metallacycle-Cored Liquid Crystals Induced by Metal Coordination. *Angew. Chem.* **2020**, *132*, 10229–10236. [CrossRef]
21. Fan, Y.; Zhang, J.; Li, Y.; Chen, Q.; Ni, Z.; Zhou, H.; Yu, J.; Qiu, H.; Yin, S. Amphiphilic Rhomboidal Metallacycles with Aggregation-Induced Emission and Aggregation-Caused Quenching Luminogens for White-Light Emission and Bioimaging. *Mater. Chem. Front.* **2022**, *6*, 633–643. [CrossRef]
22. Pollock, J.B.; Schneider, G.L.; Cook, T.R.; Davies, A.S.; Stang, P.J. Tunable Visible Light Emission of Self-Assembled Rhomboidal Metallacycles. *J. Am. Chem. Soc.* **2013**, *135*, 13676–13679. [CrossRef] [PubMed]

23. Mukherjee, P.S.; Das, N.; Kryschenko, Y.K.; Arif, A.M.; Stang, P.J. Design, Synthesis, and Crystallographic Studies of Neutral Platinum-Based Macrocycles Formed via Self-Assembly. *J. Am. Chem. Soc.* **2004**, *126*, 2464–2473. [CrossRef] [PubMed]
24. Yao, H.; Yuan, L.; Pei, L.; Shen, Y.; Zhang, Y.; Zhou, L.; Bian, H. Phosphorescent Pt(<scp>ii</scp>) Acetylacetonate Complexes Bearing 9-(Pyrimidin-2-Yl)-9 *H* -Carbazole Ligand: Syntheses, Photophysical Properties and OLED Applications. *J. Mater. Chem. C* **2023**, *11*, 16679–16688. [CrossRef]
25. Pollock, J.B.; Cook, T.R.; Schneider, G.L.; Lutterman, D.A.; Davies, A.S.; Stang, P.J. Photophysical Properties of Endohedral Amine-Functionalized Bis(Phosphine) Pt(II) Complexes as Models for Emissive Metallacycles. *Inorg. Chem.* **2013**, *52*, 9254–9265. [CrossRef] [PubMed]
26. Saha, M.L.; Yan, X.; Stang, P.J. Photophysical Properties of Organoplatinum(II) Compounds and Derived Self-Assembled Metallacycles and Metallacages: Fluorescence and Its Applications. *Acc. Chem. Res.* **2016**, *49*, 2527–2539. [CrossRef] [PubMed]
27. He, Z.; Li, M.; Que, W.; Stang, P.J. Self-Assembly of Metal-Ion-Responsive Supramolecular Coordination Complexes and Their Photophysical Properties. *Dalt. Trans.* **2017**, *46*, 3120–3124. [CrossRef] [PubMed]
28. Acharya, N.; Upadhyay, M.; Dey, S.; Ray, D. White Light Emission Achieved by Dual-TADF in a Single Emissive Layer of Multicomponent Emitters. *J. Phys. Chem. C* **2023**, *127*, 7536–7545. [CrossRef]
29. Pollock, J.B.; Cook, T.R.; Stang, P.J. Photophysical and Computational Investigations of Bis(Phosphine) Organoplatinum(II) Metallacycles. *J. Am. Chem. Soc.* **2012**, *134*, 10607–10620. [CrossRef] [PubMed]
30. Schlickum, U.; Decker, R.; Klappenberger, F.; Zoppellaro, G.; Klyatskaya, S.; Auwärter, W.; Neppl, S.; Kern, K.; Brune, H.; Ruben, M.; et al. Chiral Kagomé Lattice from Simple Ditopic Molecular Bricks. *J. Am. Chem. Soc.* **2008**, *130*, 11778–11782. [CrossRef] [PubMed]
31. Reichardt, C. Empirical Parameters of Solvent Polarity as Linear Free-Energy Relationships. *Angew. Chem. Int. Ed.* **1979**, *18*, 98–110. [CrossRef]